RESEARCH ARTICLE



Piezoelectric Properties of Three Types of PVDF and ZnO Nanofibrous Composites

Minji Kim¹ • Jintu Fan²

Received: 29 September 2020 / Accepted: 6 February 2021 © Donghua University, Shanghai, China 2021

Abstract

Piezoelectric materials are highly desirable for wearable electronics and energy harvesting. Piezoelectric PVDF/ZnO composite nanofibers are particularly desirable for their nontoxicity, breathability, and flexibility. Here, we investigated three methods of fabricating PVDF and ZnO composite nanofibers aimed at optimum piezoelectric responses. It was found, (1) adding ZnO nanorod as fillers within the PVDF nanofiber did not improve piezoelectric response due to the fact that the process made the material more dielectric; (2) ZnO nanorods on the PVDF surface increased the power output due to the combined effects of piezoelectricity of ZnO nanorods as well as the triboelectric response of the increased surface roughness; (3) electrospraying pre-synthesized ZnO nanorods on PVDF nanofibers resulted in the highest piezoelectric response due to the combined effect of the greater piezoelectricity of aligned ZnO nanorods and PVDF nanofibers, and larger triboelectric response from increased surface roughness.

Keywords Piezoelectric · PVDF · ZnO · Electrospinning · Nanorod · Nanofiber · Nanocomposite

Introduction

Piezoelectric materials have received much attention in recent years for potential applications in energy harvesting and wearable electronics [1–4]. Soft and pliable piezoelectric polymers have been studied and applied to areas where flexibility is required [5–7]. Electrospun piezoelectric nanofibrous materials are of special value for their high surface to volume ratio, breathability, flexibility, and ease of one-step fabrication without additional poling step.

Poly(vinylidene fluoride) (PVDF) is a widely used and favored piezoelectric polymer due to its high piezoelectric, ferroelectric, and pyroelectric properties as a result of its polar crystalline structure. It is also a very attractive material for wearables as it has high resistivity to common liquids and chemicals, including water, soap, and sweat [8, 9]. While

- Minji Kim mk988@cornell.edu
- ☑ Jintu Fan jin-tu.fan@polyu.edu.hk

Published online: 22 March 2021

- Department of Fiber Science and Apparel Design, Cornell University, Ithaca, NY 14853, USA
- Institute of Textiles and Clothing, Hong Kong Polytechnic University, Hung Hom, Kowloon, Hong Kong

piezoelectric polymers have desirable mechanical properties for many applications, it has significantly lower piezoelectric and dielectric properties than ceramics [10–13]. Due to this, many previous studies have attempted to combine piezoelectric polymers and ceramics to form composites [14].

Piezoelectric composites with piezoelectric polymers and ceramics have the potential of having excellent piezoelectric properties from the ceramics and desirable mechanical properties from the polymers such as flexibility and strength. This results in relatively high dielectric permittivity and breakdown strength, which are not attainable in a single-phase piezoelectric material [15]. When it comes to wearable materials, the safety of the material should be considered utmost. Consequently, piezoelectric ceramics containing heavy metal should be avoided, such as PZT. PZT is one of the most widely used piezoelectric ceramics due to its outstanding piezoelectric properties [16, 17]. However, its toxicity and environmental issue have led many researchers to seek lead-free piezoelectric materials to replace PZT [18–21].

Zinc oxide (ZnO) is one of the few lead-free piezoelectric ceramics with high interest and has proven safe to be used such as in cosmetics [22, 23]. ZnO can be grown in many different nanoscale forms without much effort, which makes it an attractive wearable material [24–29]. Although



the potential of combining ZnO with piezoelectric polymers for flexible, breathable, and high performance piezoelectric composite materials is recognized, the question of how to best combine the piezoelectric ceramics and polymer matrix should be addressed in order to achieve optimum performance [30–33]. In this study, we compared the piezoelectric properties of PVDF and ZnO composite nanofibers made from three different methods, viz. adding ZnO nanorods as fillers in the PVDF electrospinning solution, growing ZnO nanorod on the PVDF nanofibers, and electro-spraying ZnO onto the PVDF nanofibers.

Experimental Section

Electrospinning of PVDF Nanofiber Mats

In this study, PVDF pellets (Mw 180,000, Millipore Sigma, Burlington, MA, USA), N,N-dimethylformamide (DMF, Macron Fine Chemicals, Radnor, PA, USA), and acetone (Fisher Chemical, Waltham, MA, USA) were used as received. Then, 20 wt% of PVDF solution was prepared by adding PVDF pellets to the DMF-acetone solvent mixture (7/3 v/v) and stirring the solution with a magnetic stirring bar at 70 °C for 5 h. The polymer solution was loaded into a plastic syringe, and a 23-gauge needle was used as a spinneret. The flow rate was controlled at 1 mL/h with a syringe pump (PHD ULTRA, Harvard Apparatus, Cambridge, MA, USA), and a 14 kV voltage was applied by a DC power supply (Matsusada Precision, Kusatsu-shi, Japan) between the needle and a grounded metal collector with a distance of 10 cm. The needle was moved laterally with a stroke distance of 18 cm and four strokes per min. The collector was 10 cm in diameter, and the rotation speed was 200 rpm [24].

Hydrothermal Synthesis of ZnO Nanorods

Single-crystalline ZnO nanorods were prepared by the hydrothermal synthesis method in an autoclave. 20 mL of 0.1 M of a zinc acetate dihydrate (Zn(Ac) $_2$ ·2H $_2$ O) solution in ethanol and 40 mL of 0.5 M sodium hydroxide (NaOH) in ethanol was transferred to a Teflon-lined stainless steel autoclave and heated at 150 °C for 15 h [34]. The solution with white precipitate was vacuum filtered with 0.4 μ m membranes.

Electrospinning of PVDF Nanofiber Mats with ZnO Nanorod Fillers

PVDF with a ZnO filler solution consisted of 20 wt% of PVDF, and the ZnO filler amount was 5 wt% of PVDF. First, ZnO nanorods were added to the DMF-acetone solvent mixture (7/3 v/v) and then sonicated for 90 min. After

sonication, PVDF pellets were added and stirred with a magnetic stirring bar at 70 °C for 5 h.

Electrospraying of ZnO Nanorods onto PVDF Nanofiber Mat

10 mL of 1.5 wt% ZnO nanorods in water was sonicated for 90 min and then electrosprayed onto PVDF nanofiber mats on the collector. The flow rate was 10 mL/h, and the rest of the parameters were the same as the electrospinning process for PVDF.

Hydrothermal Growth of ZnO Nanorods

In previous research, we have demonstrated the successful growth of ZnO on a PVDF nanofiber surface [24]. The hydrothermal growth method of ZnO nanorods on PVDF nanofiber was modified from a similar growth method on cotton or nylon microfibers [25, 35-37]. First, solution concentration was diluted more than those in previously reported methods, thus resulting in smaller nanorods that would be in the range of nanofiber diameter. Second, the seeding step was repeated three times to produce nucleation sites on a more chemically inert PVDF fiber surface than nylon or cotton [37]. Third, the reaction temperature was lowered to 60 °C to prevent the heat relaxation of semi-crystalline PVDF nanofibers [38]. Finally, equimolar amounts of hexamethylenetetramine and zinc nitrate hexahydrate in the growth solution were replaced by a higher concentration of hexamethylenetetramine to yield the preferred ratio of the length to the diameter of ZnO crystals [36, 39].

ZnO Seed Solution

The ZnO seed solution was prepared in 50 mM concentration and diluted to 10 mM before use. Zinc acetate dihydrate (Zn(Ac)₂·2H₂O, 1.6462 g) was dissolved in 150 mL of isopropyl alcohol at 85 °C with a vigorous stir at 1000 rpm for 17 min. Triethylamine (N(CH₂CH₃)₃, 0.7637 g) was added dropwise to the solution and stirred again at 85 °C, 400 rpm for 13 min. The resulting 50 mM seed solution was incubated at room temperature without stirring for 6 h [24].

ZnO Growth Solution

The growth solution was prepared in 100 mM concentration and diluted to 10 mM before use. Hexamethylenetetramine $(C_6H_{12}N_4, 9.3457~g)$ was dissolved in 400 mL of room-temperature deionized (DI) water, and the solution was stirred for 10 min. Zinc nitrate hexahydrate $(Zn(NO_3)_2, 11.8991~g)$ was added to the solution and stirred for 24 h [24].



Growth of ZnO Nanorods on PVDF Fiber Surfaces

During the seeding step of ZnO deposition, it is desired to form hexagonal nanorods arranged vertically to the substrate surface for the maximum strain rate transfer [35]. Therefore, the seeding process was repeated three times to provide sufficient nucleation sites [24, 37]. The oven temperature for seed curing and growth process was lowered to 60 °C and duration to 6 h to inhibit the heat relaxation of PVDF and preserve the polarization of the electrospun fibers, thus avoiding an additional poling process [38].

Characterization

Field-emission scanning electron microscope (FESEM) images were taken using a Gemini 500 microscope (ZEISS, Oberkochen, Germany) with an accelerating voltage of 1 keV. To extract the detailed geometry with better focus and reduce the charging effect under a FESEM, the samples were sputter coated with palladium/gold. The average PVDF fiber diameter and ZnO nanorod length and diameter were determined using FESEM images over 30 fibers with the ImageJ software (NIH, Bethesda, Rockville, MD, USA) [40].

The crystallography of PVDF nanofibers and ZnO nanorods was examined by X-ray diffraction (XRD) with the theta-theta diffractometer (D8 GADDS, Bruker), Cu- $K\alpha$ radiation (= 1.54 Å) at a 0.02° scanning step and an operating voltage of 40 kV and a current of 40 mA were used.

Fourier-transform infrared (FTIR) spectroscopy from 4000 to 650 cm⁻¹ (Frontier FTIR, PerkinElmer, Waltham, MA, USA) was performed at room temperature to evaluate the polymer crystalline phase; FTIR spectra were collected with 16 scans and a resolution of 4 cm⁻¹.

Thermal gravimetric analyses (TGA) were used to determine the thermal stability, and the amount of ZnO added to PVDF nanofibers (Q500 Thermogravimetric Analyzer, TA Instruments, New Castle, DE, USA) by the heat removal of PVDF. Samples were heated up from room temperature to 990 °C with the rate of 10 °C/min on a ceramic pan under a nitrogen ambient.

Piezoelectric Testing

The piezoelectric testing module was assembled by sandwiching the piezoelectric nanofiber mat between two electrodes made by conductive fabric (cotton and silver blend double jersey knit purchased from LessEMF, Latham, NY, USA). Wires were connected to the electrodes using conductive ink and epoxy.

The piezoelectric performance of the electrospun samples was evaluated by periodic tensile testing in a customized

setup with a motorized actuator controlled by a controller and a module (ni-cRIO 9036 and ni-9503, National Instruments, Austin, TX, USA), a pressure sensor (LC201-300/N, Newport Electronics, Santa Ana, CA, USA), an electrometer (6517B, Keithley Instruments, Cleveland, OH, USA), a multimeter (34470A, Keysight, Santa Rosa, CA, USA), a source meter (2400, Keithley, Cleveland, OH, USA), and a programmable DC power supply (9130, BK Precision, Yorba Linda, CA, USA). The open-circuit voltage was measured with a Keithley 6517B electrometer, and the closed-circuit current was measured with a Keithley 2400 source meter. The testing head movement was set to 1 Hz, and the impact pressure was set to 0.10 MPa, which is within the human foot pressure range of 0–0.20 MPa [41–43], although the applications are not limited to shoes. LabView software (National Instruments, Austin, TX, USA) was used to control all the components and record voltage and current outputs synchronously.

Results and Discussion

Material Analysis

The amount of ZnO added in the three composites was controlled to be close to 6 wt%. In our previous work on developing the method to grow ZnO nanorods on PVDF nanofiber surface [24], one of the main focuses was to prevent heat relaxation of PVDF, which would decrease in β -phase percentage. The ZnO growth amount from this method was 6 wt%, which became our control amount. A longer time or higher temperature of ZnO growth condition would yield a higher content of ZnO nanorods. However, it would also result in heat relaxation of the crystalline region of PVDF, including the β -phase. Also, a higher ZnO content in composites could result in higher power output. However, ZnO overload can cause a brittle composite material from but not limited to the formation of ZnO clusters.

Thermalgravimetric analysis (TGA) and its derivative (DTG) are widely used to characterize the thermal stability of polymeric materials and its inorganic content percent. In Fig. 1a and b, TGA and DTG of as-spun PVDF nanofibers and three composites—PVDF fibers with ZnO fillers (ZnO+PVDF), ZnO nanorods grown on the fiber surface (ZnO@PVDF), and electrosprayed on the nanofiber mat surface (ZnO/PVDF)—were examined. The ZnO weight percentage of the ZnO+PVDF was 6.36 wt%, the ZnO@PVDF was 6.23 wt%, and the ZnO/PVDF was 6.20 wt%.

TGA graph shows that PVDF goes through two-step degradation. The first step occurs at 440–480 °C, and the second one occurs at 480–950 °C. The decomposition mechanism of the first degradation step is a chain-stripping process. In this process, the pristine polymers' destruction occurs where



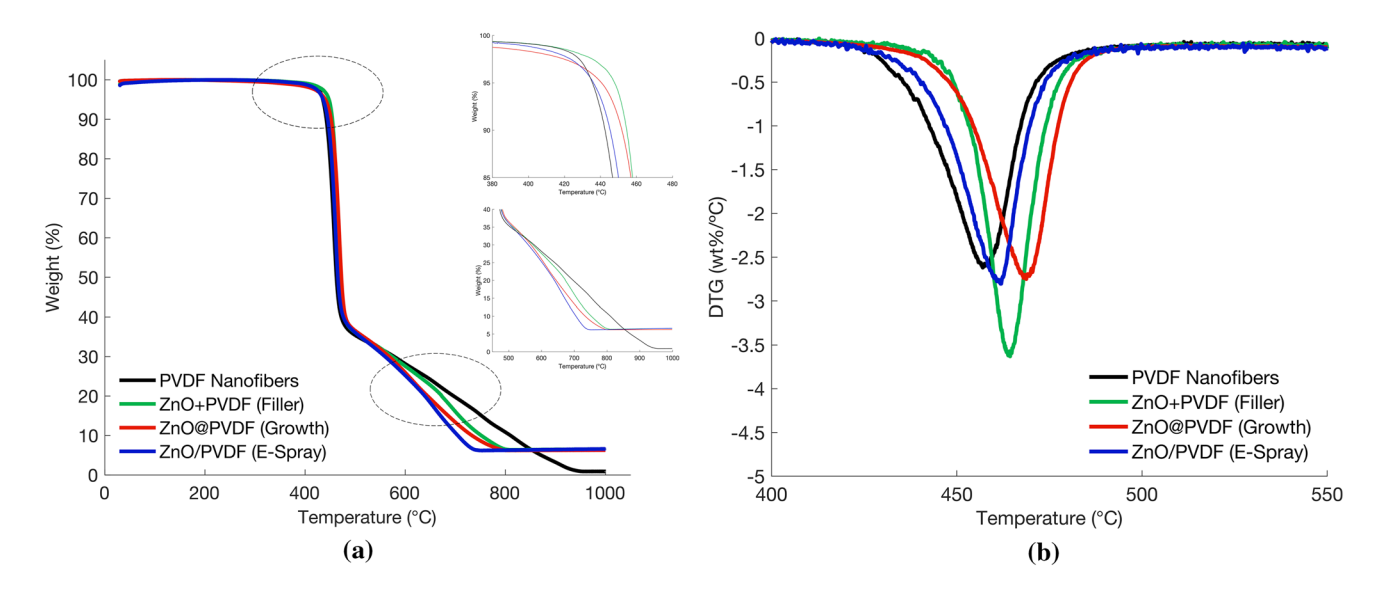


Fig. 1 (a) TGA and (b) DTG curves of the PVDF membrane, ZnO+PVDF, ZnO@PVDF, and ZnO/PVDF

the carbon–hydrogen and carbon–fluorine bonds undergo scission, and conjugated systems form [44, 45]. During the second step, the unstable polyenic sequence from the first step undergoes reactions and leads to scission followed by aromatic molecules' formation [44, 46].

A slight increase at the start of the first degradation step temperature with ZnO nanorod addition has been observed. Thermal degradation temperature for 10% weight loss was 442 °C for as-spun PVDF, 445 °C for ZnO/PVDF, 452 °C for ZnO@PVDF, and 455 °C for ZnO+PVDF. The filler addition method resulting in the highest PVDF degradation onset temperature may be related to having the most interaction between PVDF and ZnO materials. The thermal stability of the nanofiber membranes increases when there is an interaction between nanorods and polymers [47].

As the second step progresses, as-spun PVDF degraded slowest, followed by filler (ZnO+PVDF), growth (ZnO@PVDF), and e-spun (ZnO/PVDF) composites. This was clear with the temperature at thermal degradation for 90% weight loss. It was 810 °C for as-spun PVDF, 705 °C for ZnO/PVDF, 734 °C for ZnO@PVDF, and 752 °C for ZnO+PVDF. ZnO nanorods hindered aromatic molecules' formation during this step, thus as-spun PVDF resulted in the slowest degradation. Between ZnO and PVDF composites, degradation may be slower as the interaction between the two materials is stronger.

The first derivative of the weight percentage difference versus the degradation temperature has been analyzed as well (Fig. 7b). Inflection temperature is the temperature at which the mass loss rate is maximum, and it was higher with composites with ZnO than pure PVDF. This confirmed

the enhanced thermal stability from the interaction between ZnO and PVDF.

The morphology of PVDF nanofibers and the three composites were examined using a FESEM and shown in Fig. 2. Morphology of the three composites are different, but the interaction of PVDF and ZnO are alike. Major interactions between PVDF and ZnO are mechanical entanglements, Van der Waals force and hydrogen bonds [48, 49]. Mechanical force (viz. entanglements and Van der Waals force) increases as the material size gets smaller and the aspect ratio gets more extensive. Interfacial force is most potent with the fillers as it shares the most interfacial area by being encapsulated with PVDF. We found that the binding of PVDF nanofibers and ZnO Nanorods through mechanical force and hydrogen bonds are sufficient to withstand the subsequent water rinse.

FESEM images show that ZnO@PVDF (Fig. 2c) and ZnO/PVDF (Fig. 2d) clearly have more nanoscale surface roughness than that of as-spun PVDF (Fig. 2a) and ZnO+PVDF (Fig. 2b). The nanoscale roughness structure is known to contribute to the triboelectric effect, producing friction and increasing the surface charges [6, 50, 51].

Figure 3 shows the average of the measured diameter of the PVDF nanofiber and the ZnO nanorod diameter and length with error bars with one standard deviation.

It can be seen from Fig. 3a, adding ZnO as fillers in electrospun PVDF nanofiber reduces the diameter of the nanofibers distinctly. Such a morphological difference is contributed from the increase in conductivity values of the polymer solution with nanofillers and resulted in finer fibers [52–55].



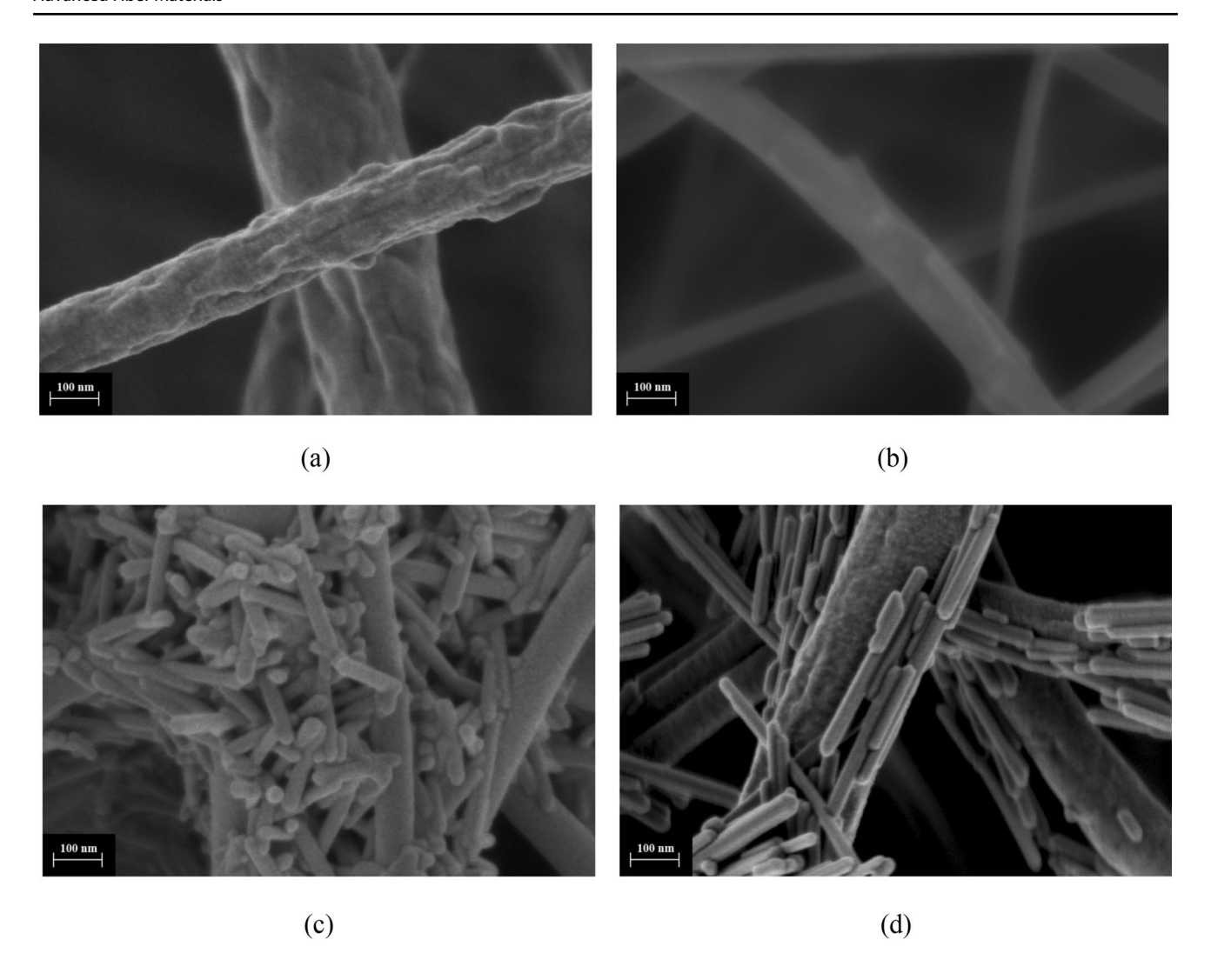


Fig. 2 FESEM images of the (a) electrospun PVDF nanofibers; (b) ZnO nanorod fillers in PVDF nanofibers (ZnO+PVDF); (c) ZnO growth on a PVDF nanofiber surface (ZnO@PVDF); (d) ZnO nanorods electrosprayed onto PVDF nanofiber mats (ZnO/PVDF)

ZnO nanorods grown on the surface of PVDF (ZnO@ PVDF) and ZnO nanorods used for fillers or electrospraying (ZnO+PVDF or ZnO/PVDF) were controlled to have similar diameters. This resulted in a slight difference in the length of the two types of ZnO nanorods due to the different synthesis methods. The ZnO nanorods pre-synthesized separately had an average length of 228 nm. Whereas ZnO grown on the PVDF surface had an average length of 142 nm. The pre-synthesis of ZnO nanorods was carried out at 150 °C, whereas the growth of ZnO nanorods was carried out at 60 °C. At a relatively lower temperature, the growth increases more along the thickness-wise < 2 11 0 > rather than length-wise < 0001 > direction [56] and, therefore, the ZnO nanorods synthesized in higher temperature resulted in a slightly longer length. Synthesizing ZnO nanorods separately have more possibility of controlling the morphology from the ease of changing the parameters such as solution concentration, temperature, and duration. Growing ZnO nanorod on PVDF fibers has a temperature and duration limit in order to not depolarize PVDF [24]. Wurtzite-structured ZnO has the polarization direction along the c-axis and has the preferential growth along the c-axis direction to minimize the free energy of the entire reaction system [57]. Previous researchers have identified the length of ZnO nanorods' impact on the piezoelectric voltage output of nanogenerators [58, 59]. Therefore, a longer ZnO nanorod is preferred as it would have a higher piezoelectric response in compression and elastic deformation [60, 61].

The FTIR spectra were studied to analyze the PVDF crystalline phases as-pun, with ZnO fillers, after the ZnO hydrothermal growth process, and ZnO electrospraying. Figure 4 compares the FTIR spectra of the electrospun PVDF nanofibers and the three composites. Each spectrum was normalized by a signal of an internal standard



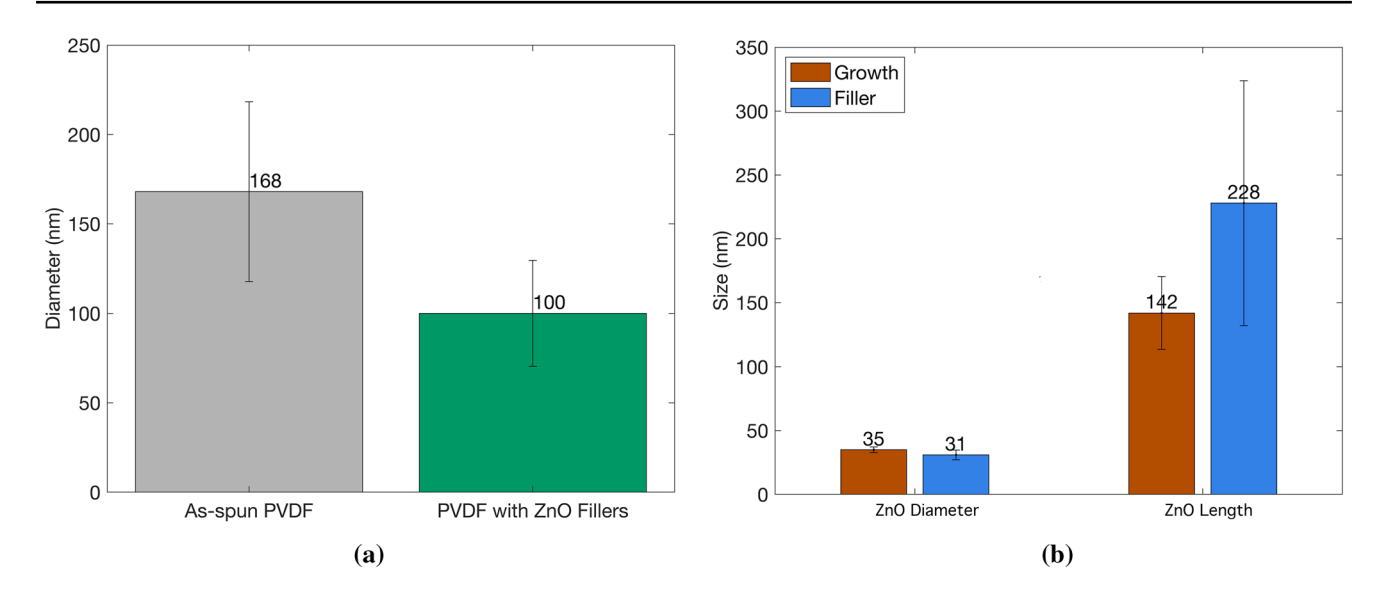


Fig. 3 (a) Nanofiber diameter average of electrospun PVDF and PVDF with ZnO fillers. (b) ZnO nanorods' diameter and length average comparison with hydrothermal growth method at $60~^{\circ}$ C and pre-synthesized at $150~^{\circ}$ C

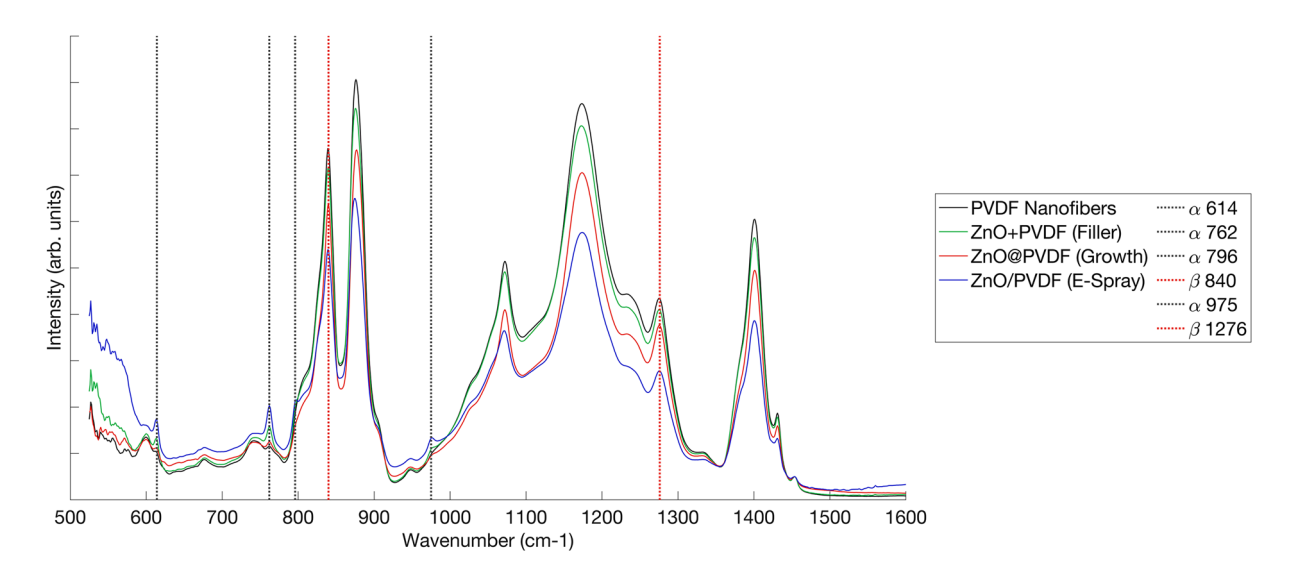


Fig. 4 FTIR spectra showing the effect of the three ZnO nanorod addition methods to PVDF crystalline phases

at 1,454 cm⁻¹, corresponding to the CH₂ in-plane bending [62]. All samples exhibit two strong polar β crystalline peaks at 840 cm⁻¹ (β , CH2 rocking) and 1,276 cm⁻¹ (β , CF out-of-plane deformation), and weak, non-polar, α crystalline peaks at 614 cm⁻¹ (α , CF₂ bending and skeletal bending), 762 cm⁻¹ (α , CF₂ bending), 796 cm⁻¹ (α , CF₂ rocking), and 975 cm⁻¹ (α , CH out-of-plane deformation) [63, 64]. The effects of fillers, hydrothermal growth, and electrospraying of ZnO nanorods on PVDF β crystals were considered by the intensity of the α and β crystalline peaks. None of the samples changed dramatically in terms of the intensity of the

 α and β crystalline peaks. Furthermore, the β -phase percentage can be quantified using the following equation:

$$F_{\beta} = \frac{X_{\beta}}{X_{\alpha} + X_{\beta}} = \frac{A_{\beta}}{(K_{\beta}/K_{\alpha})A_{\alpha} + A_{\beta}} \tag{1}$$

where F_{β} represents the PVDF β-phase percentage, A_{α} and A_{β} denote their absorption bands at 762 and 840 cm⁻¹, and K_{α} and K_{β} are the absorption coefficients at the respective wavenumbers, which are 6.1×10^4 and 7.7×10^4 cm²·mol⁻¹, respectively [64–66]. The calculated β-phase percentage for the electrospun PVDF nanofibers was 83.7%, 78.2% for



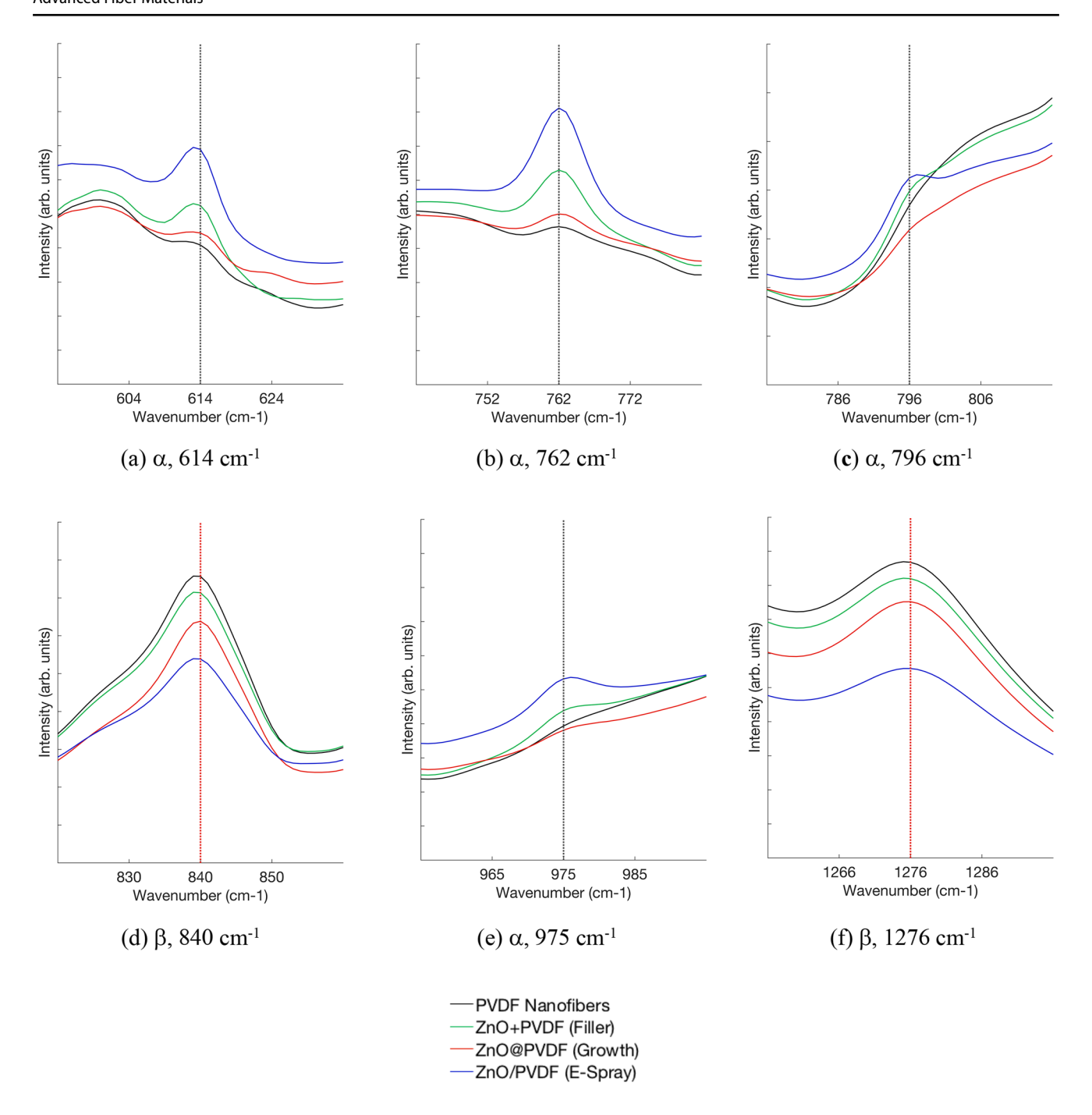


Fig. 5 Peaks of FTIR spectra corresponding to α and β crystalline phases of PVDF: (a) α , 614 cm⁻¹; (b) α , 762 cm⁻¹; (c) α , 796 cm⁻¹; (d) β , 840 cm⁻¹; (e) α , 975 cm⁻¹; and (f) β , 1276 cm⁻¹

ZnO+PVDF, 80.1% for ZnO@PVDF, and 67.8% for ZnO/PVDF. Electrospraying ZnO nanorods resulted in a relatively lower β -phase percentage, whereas applying ZnO nanorods as fillers and growing on the surface of PVDF did not change the β -phase percentage significantly.

The relatively lower β -phase percentage for ZnO/PVDF may be due to the fact that, in the process of electrospraying ZnO nanorods, the electric field was applied to the PVDF

membrane in the membrane thickness direction at room temperature. The net dipole of piezoelectric PVDF nanofibers, which are in the fiber axis direction, could be reduced by applying a field in a different direction to the dipole direction at room temperature [67]. The net dipole of piezoelectric PVDF nanofibers is in the fiber axis direction because electrospinning parameters leading to a higher stretching of the jet is known to be the major contribution of the electroactive



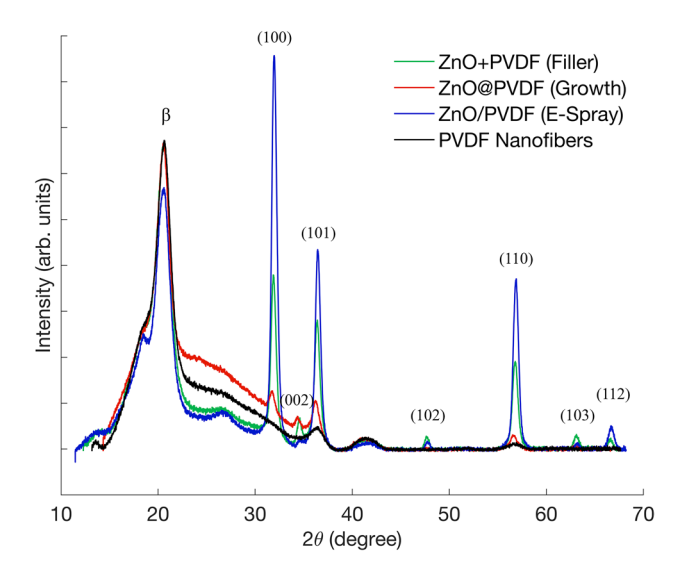


Fig. 6 XRD spectra of the PVDF membrane and three types of ZnO and PVDF composites

β-phase than electric poling [68, 69]. Drawing and electrical poling are the two methods that could transition PVDF's α-phase to β-phase during electrospinning [12, 70–73]. Mechanical drawing contributes to the transition of the original spherulitic structure into a crystal array, in which the molecules are forced into their most extended conformation (polar β-phase), with all of the dipole moments aligned in the same direction [74–76]. Therefore, an external electric field perpendicular to the fiber axis during electrospraying partially reduced the PVDF net dipole.

The ZnO fillers in the PVDF may have affected β -phase content by influencing the crystallization of PVDF. It has been reported that fillers in PVDF polymer matrixes have a nucleating effect at low levels, 1–5 wt%. However, above these levels, the degree of crystallinity decreases as fillers hinder the crystallization [77, 78]. Hydrothermal growth least affected the β -phase percentage, and a small difference is suspected to be from the heat relaxation of the crystalline region of PVDF [24, 38]. From the comparison of the FTIR spectra, it can be concluded that the electrospraying step depolarized the PVDF nanofibers the most, and the hydrothermal growth of ZnO did the least (Fig. 5).

Figure 6 displays the X-ray diffraction patterns of the electrospun PVDF nanofibers and the three types of ZnO

and PVDF composite nanofibers. The electrospun PVDF nanofibers exhibited strong peak 2θ values at 20.4°, which corresponds to the β-phase crystalline. Three ZnO and PVDF composite nanofibers have reflection peaks at 2θ values of 31.9° (100), 34.5° (002), 36.4° (101), 47.7° (102), 56.8° (110), 63.1° (103), and 66.7° (112), which can be indexed as the hexagonal wurtzite structure [79, 80]. No diffraction peaks from any other impurity phases were found, confirming that only single-phase hexagonal ZnO was present. Peaks corresponding to the (100), (002), (101), (102), (110), (103), and (112) planes of ZnO confirmed the successful incorporation of ZnO wurtzite crystals to the PVDF matrix [81, 82]. There was no significant difference in the PVDF α and β crystalline peak with the ZnO+PVDF and the ZnO@PVDF composite, whereas the ZnO/PVDF composite's β crystalline peak decreased slightly, which corresponds with the FTIR spectra results.

Piezoelectric Measurements

The piezoelectric testing module of PVDF and its composites were assembled by sandwiching the piezoelectric nanofiber mat between two electrodes made by conductive fabric. Figure 7 shows a schematic illustration of the breathable fibrous nanogenerator. Wires were connected to the electrodes using conductive ink and epoxy. No external casing was used to maintain the assembly's breathability, which resulted in a permeable assembly between the electrodes and the membrane [24].

Short-circuit is when the circuit's resistance is zero, and a closed-circuit is when there is considerable resistance. An open-circuit is the opposite of a short-circuit where there is an infinitely high resistance such as a disconnection. The nanogenerators' closed-circuit currents with different resistive loads were compared, and the closed-circuit voltages and the power density were derived accordingly. Table 1 lists the average values of the maximum peak currents with resistive loads of 0.47, 15, 30, and 60 M Ω . Figure 8a shows the nanogenerator load curve with all the data points from the different loads. Nonlinear least-square fitting was performed using the following equation:

$$V = V_{oc} \left(1 - \exp\left(\left(I - I_{sc} \right) / I_0 \right) \right) \tag{2}$$

Fig. 7 The schematic illustration of the breathable fibrous nanogenerator

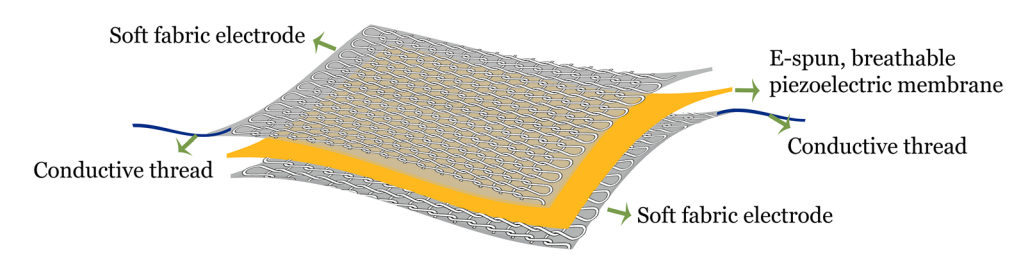




Table 1 Comparison of closed-circuit current and voltages of electrospun PVDF and three different types of ZnO and PVDF nanofiber composites

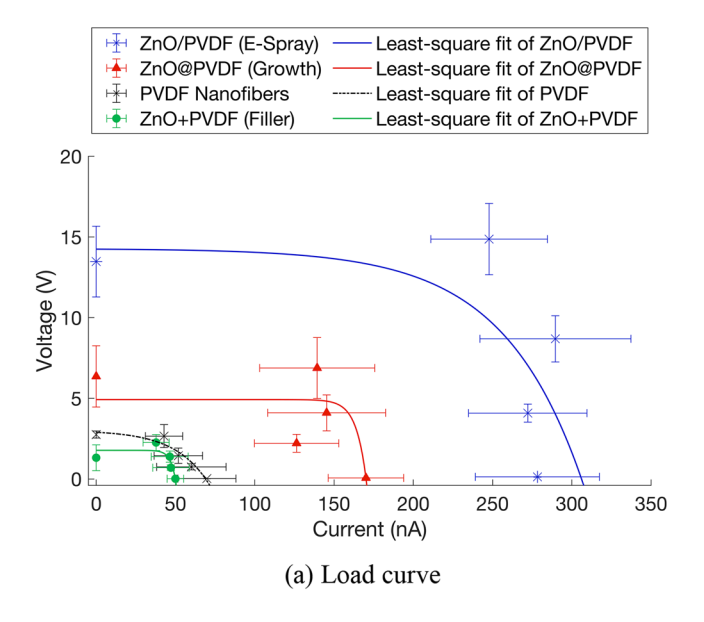
	0.47 ΜΩ	15 ΜΩ	30 ΜΩ	60 MΩ
PVDF				
Current (nA)	54.01	50.26	48.25	44.36
Power density (nW/cm ²)	0.09	2.53	4.66	7.87
Voltage (V)	0.025	0.754	1.447	2.661
Standard deviation $\sigma(V)$	0.007	0.190	0.470	0.708
Coefficient of variation	0.29	0.25	0.32	0.27
ZnO@PVDF				
Current (nA)	136.88	147.66	136.69	114.67
Power density (nW/cm ²)	0.59	31.80	37.37	52.60
Voltage (V)	0.064	2.215	4.101	6.880
Standard deviation $\sigma(V)$	0.016	0.553	1.111	1.886
Coefficient of variation	0.25	0.25	0.27	0.27
ZnO/PVDF				
Current (nA)	278.26	272.19	289.62	247.81
Power density (nW/cm ²)	2.43	74.09	167.76	245.63
Voltage (V)	0.131	4.083	8.689	14.868
Standard deviation $\sigma(V)$	0.018	0.560	1.430	2.205
Coefficient of variation	0.14	0.14	0.16	0.15
ZnO + PVDF				
Current (nA)	49.91	47.10	46.35	37.70
Power density (nW/cm ²)	0.08	2.22	4.30	5.69
Voltage (V)	0.023	0.706	1.391	2.262
Standard deviation $\sigma(V)$	0.002	0.172	0.348	0.495
Coefficient of variation	0.10	0.24	0.25	0.22

where V represents the measured voltage, I denotes the measured current, and V_{oc} , I_{sc} , and I_0 are the extracted parameters of the open-circuit voltage, short-circuit current, and I-V sharpness fitting, respectively. Figure 8b displays the typical transient current responses when the sample was subjected to cyclic compressive impacts with a resistive load of 15 $M\Omega$.

As seen in Table 1, Fig. 8, the ZnO/PVDF produced the highest power output, with the ZnO@PVDF being the second highest; the ZnO+PVDF was lower than the as-spun PVDF.

ZnO+PVDF composite's lower power output is in alignment with some previous works on ZnO fillers enhancing dielectric constant of polymer composite materials, including PVDF [49, 83]. Additionally, ZnO hindered the crystallization of PVDF during electrospinning, as discussed with FTIR data (Table 2).

The added triboelectric effect most likely caused the increased voltage output of ZnO@PVDF and ZnO/PVDF due to the increased surface roughness. Past research has shown that increased roughness and high specific surface area can induce a high surface charge density for triboelectricity [84]. As shown by the FESEM images in Fig. 2, having ZnO nanorods on the surface substantially increases surface roughness of ZnO@PVDF and ZnO/PVDF. Comparing ZnO@PVDF and ZnO/PVDF composites, although they have similar surface roughness and thus similar triboelectric effects, e-spraying in ZnO/PVDF composites resulted in the dipole alignment of the fiber and ZnO nanorods, generating a greater piezoelectric response. On the contrary,



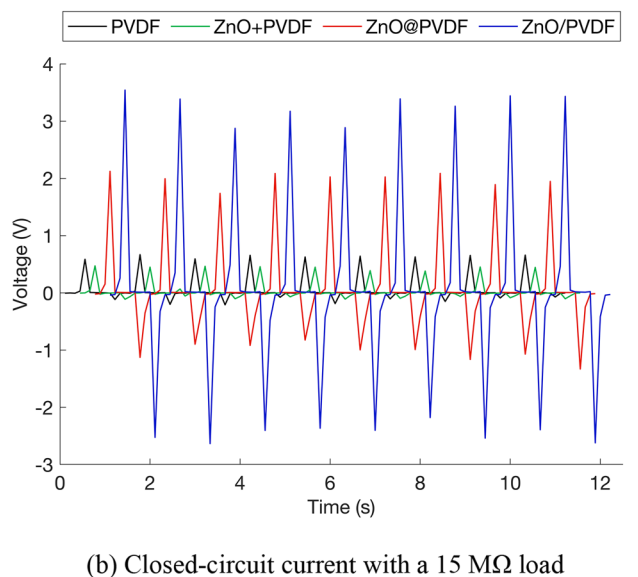


Fig. 8 Nanogenerator characteristics of 15 cm² fiber mats: (a) load curves with resistive loads of 0.47, 15, 30, and 60 MΩ; and (b) voltage from measured transient closed-circuit current measurements with a 15 MΩ resistive load (V=IR)

Table 2 Comparison of three different types of ZnO and PVDF nanofiber composites

	PVDF	ZnO@PVDF	ZnO/PVDF	ZnO+PVDF
ZnO content (%)		6.23	6.20	6.36
10% weight loss temperature (°C)	442	452	445	455
90% weight loss temperature (°C)	810	734	705	752
Fiber diameter (nm)	168			100
ZnO diameter (nm)		35	31	31
ZnO length (nm)		142	228	228
β-phase percentage (%)	83.7	80.1	67.8	78.2
Short-circuit current (nA)*	69.4	170.2	306.1	49.4
Open-circuit voltage (V)*	2.9	5.3	14.3	1.8

^{*}Extracted parameters

the dipoles of fibers and ZnO in the ZnO@PVDF composite were mostly perpendicular.

Conclusions

The piezoelectric properties of three types of electrospun PVDF nanofibers and ZnO nanorod composites were investigated and compared. The amount of ZnO in the three different composites was controlled to be the same. It was found, (1) adding ZnO nanorod as fillers within the PVDF nanofiber does not improve piezoelectric response. However, the fillers made the materials more dielectric, hindered the crystallization of PVDF, and resulted in lower power output; (2) ZnO nanorods on the PVDF surface (ZnO/PVDF or ZnO@ PVDF) increased the power output due to the combined effects of piezoelectricity of ZnO nanorods as well as the triboelectric response of the increased surface roughness; (3) ZnO/PVDF had the highest piezoelectric response despite the relatively lower β-phase percentage caused by the different direction of the PVDF polarization and the electric field in electrospraying. This is due to the triboelectric effect from the surface roughness and higher piezoelectric effect from the ZnO axis alignment with the PVDF fiber axis. In this study we have controlled the composites' ZnO content to 6 wt% due to the limitation of the ZnO hydrothermal growth method's temperature and duration. Further optimization of the ZnO quantity of the e-spray method may be explored in future research.

Acknowledgements This work made use of the Cornell Center for Materials Research Shared Facilities which are supported through the NSF MRSEC program (DMR-1719875).

Compliance with ethical standards

Conflict of interest On behalf of all authors, the corresponding author states that there is no conflict of interest.

References

- Anton SR, Sodano HA. A review of power harvesting using piezoelectric materials (2003–2006). Smart Mater Struct. 2007;16:R1.
- Hu Y, Wang ZL. Recent progress in piezoelectric nanogenerators as a sustainable power source in self-powered systems and active sensors. *Nano Energy*. 2015;14:3–14.
- Tao X. Smart fibres, fabrics and clothing: fundamentals and applications. NY: Elsevier; 2001.
- Kim I, Shahariar H, Ingram WF, Zhou Y, Jur JS. Inkjet process for conductive patterning on textiles: maintaining inherent stretchability and breathability in knit structures. *Adv Funct Mater*. 2019;29:1807573.
- Zhang M, Gao T, Wang J, et al. A hybrid fibers based wearable fabric piezoelectric nanogenerator for energy harvesting application. *Nano Energy*. 2015:13:298–305.
- Huang T, Wang C, Yu H, Wang H, Zhang Q, Zhu M. Human walking-driven wearable all-fiber triboelectric nanogenerator containing electrospun polyvinylidene fluoride piezoelectric nanofibers. *Nano Energy*. 2015;14:226–35.
- 7. Stoppa M, Chiolerio A. wearable electronics and smart textiles: a critical review. *Sensors*. **2014**;*14*:11957–92.
- Chang J, Dommer M, Chang C, Lin L. Piezoelectric nanofibers for energy scavenging applications. *Nano Energy*. 2012;1:356–71.
- 9. Lovinger AJ. Ferroelectric polymers. *Science*. **1983**;220:1115–21.
- Kochervinskii VV, Kozlova NV, Khnykov AY, Shcherbina MA, Sulyanov SN, Dembo KA. Features of structure formation and electrophysical properties of poly(vinylidene fluoride) crystalline ferroelectric polymers. *J Appl Polym Sci.* 2010;116:695–707.
- Tichý PJ, Erhart DJ, Kittinger PDE, Přívratská PJ. Piezoelectric materials. In: Fundamentals of piezoelectric sensorics. Berlin: Springer; 2010. p. 119–85.
- 12. Harrison JS, Ounaies Z. Piezoelectric polymers. *Encycl Polym Sci Technol*. **2002**. https://doi.org/10.1002/0471440264.pst427.
- Wang X, Shi J. Piezoelectric nanogenerators for self-powered nanodevices. In: Piezoelectric nanomaterials for biomedical applications. Berlin: Springer; 2012. p. 135–72.
- He F-A, Kim M-J, Chen S-M, Wu Y-S, Lam K-H, Chan HL-W, Fan J-T. Tough and porous piezoelectric P(VDF-TrFE)/organosilicate composite membrane. *High Perform Polym.* 2017;29:133–40.
- Jain A, Pk J, Sharma AK, Jain A, Pn R. Dielectric and piezoelectric properties of PVDF/PZT composites: a review. *Polym Eng Sci.* 2015;55:1589–616.
- Kang M-G, Jung W-S, Kang C-Y, Yoon S-J. Recent progress on PZT based piezoelectric energy harvesting technologies. *Actua-tors*. 2016;5:5.



- Swallow LM, Luo JK, Siores E, Patel I, Dodds D. A piezoelectric fibre composite based energy harvesting device for potential wearable applications. Smart Mater Struct. 2008;17:025017.
- Panda PK. Review: environmental friendly lead-free piezoelectric materials. J Mater Sci. 2009;44:5049–62.
- Matsubara M, Yamaguchi T, Sakamoto W, Kikuta K, Yogo T, Hirano S. Processing and piezoelectric properties of lead-free (K, Na) (Nb, Ta) O3 ceramics. J Am Ceram Soc. 2005;88:1190–6.
- Jung W-S, Kang M-G, Moon HG, Baek S-H, Yoon S-J, Wang Z-L, Kim S-W, Kang C-Y. High output piezo/triboelectric hybrid generator. Sci Rep. 2015;5:9309.
- 21. Maeder MD, Damjanovic D, Setter N. Lead free piezoelectric materials. *J Electro.* **2004**;*13*:385–92.
- Schilling K, Bradford B, Castelli D, Dufour E, Frank Nash J, Pape W, Schulte S, Tooley I, van den Bosch J, Schellauf F. Human safety review of "nano" titanium dioxide and zinc oxide. *Photochem Photobiol Sci.* 2010;9:495–509.
- Newman MD, Stotland M, Ellis JI. The safety of nanosized particles in titanium dioxide
 – and zinc oxide
 –based sunscreens. *J Am Acad Dermatol.* 2009;61:685
 –92.
- Kim M, Wu YS, Kan EC, Fan J. Breathable and flexible piezoelectric ZnO@PVDF fibrous nanogenerator for wearable applications. *Polymers.* 2018;10:745.
- Athauda TJ, Ozer RR. Nylon fibers as template for the controlled growth of highly oriented single crystalline ZnO nanowires. *Cryst Growth Des.* 2013;13:2680–6.
- Koka A, Zhou Z, Sodano HA. Vertically aligned BaTiO3 nanowire arrays for energy harvesting. *Energy Environ Sci.* 2013;7:288–96.
- Magrez A, Vasco E, Seo JW, Dieker C, Setter N, Forró L. Growth of single-crystalline KNbO3 nanostructures. *J Phys Chem B*. 2006;110:58–61.
- Jung JH, Lee M, Hong J-I, Ding Y, Chen C-Y, Chou L-J, Wang ZL. Lead-free NaNbO3 nanowires for a high output piezoelectric nanogenerator. ACS Nano. 2011;5:10041–6.
- Schmidt-Mende L, MacManus-Driscoll JL. ZnO nanostructures, defects, and devices. *Mater Today*. 2007;10:40–8.
- Zeng W, Tao X-M, Chen S, Shang S, Wah Chan HL, Hong Choy S. Highly durable all-fiber nanogenerator for mechanical energy harvesting. *Energy Environ Sci.* 2013;6:2631–8.
- Lee M, Chen C-Y, Wang S, Cha SN, Park YJ, Kim JM, Chou L-J, Wang ZL. A hybrid piezoelectric structure for wearable nanogenerators. Adv Mater. 2012;24:1759–64.
- 32. Nunes-Pereira J, Sencadas V, Correia V, Rocha JG, Lanceros-Méndez S. Energy harvesting performance of piezoelectric electrospun polymer fibers and polymer/ceramic composites. *Sens Actuator A Phys.* **2013**;196:55–62.
- Kang HB, Han CS, Pyun JC, Ryu WH, Kang C-Y, Cho YS. (Na, K)NbO3 nanoparticle-embedded piezoelectric nanofiber composites for flexible nanogenerators. *Compos Sci Technol*. 2015;111:1–8.
- Cheng B, Samulski T. Hydrothermal synthesis of one-dimensional ZnO nanostructures with different aspect ratios. *Chem Comm.* 2004:10:986–7.
- Athauda TJ, Neff JG, Sutherlin L, Butt U, Ozer RR. Systematic study of the structure-property relationships of branched hierarchical TiO2/ZnO nanostructures. ACS Appl Mater Interf. 2012;4:6917–26.
- Xu S, Wang ZL. One-dimensional ZnO nanostructures: solution growth and functional properties. *Nano Res.* 2011;4:1013–98.
- Baruah S, Thanachayanont C, Dutta J. Growth of ZnO nanowires on nonwoven polyethylene fibers. *Sci Technol Adv Mater*. 2008;9:025009.
- Kolbeck AG. Aging of piezoelectricity in poly(vinylidene fluoride). J Polym Sci Polym Phys Ed. 1982;20:1987–2001.

- Sugunan A, Warad HC, Boman M, Dutta J. Zinc oxide nanowires in chemical bath on seeded substrates: role of hexamine. *J Sol-Gel Sci Technol*. 2006;39:49–56.
- Rueden C, Dietz C, Horn M, Schindelin J, Northan B, Berthold M, Eliceiri K. ImageJ Ops [Software]. In: ImageJ. https://imagej. net/ImageJ Ops.
- 41. Lord M. Foot pressure measurement: a review of methodology. *J Biomed Engng.* **1981**;3:91–9.
- Urry S. Plantar pressure-measurement sensors. *Meas Sci Technol*. 1999;10:R16.
- Duckworth T, Betts RP, Franks CI, Burke J. The measurement of pressures under the foot. Foot Ankle. 1982;3:130–41.
- Jaleh B, Jabbari A. Evaluation of reduced graphene oxide/ZnO effect on properties of PVDF nanocomposite films. *Appl Surf Sci.* 2014;320:339–47.
- Chipara M, Lozano K, Hernandez A, Chipara M. TGA analysis of polypropylene–carbon nanofibers composites. *Polym Degrad Stab.* 2008;93:871–6.
- Martins P, Costa CM, Benelmekki M, Botelho G, Lanceros-Méndez S. Interface characterization and thermal degradation of ferrite/poly(vinylidene fluoride) multiferroic nanocomposites. J Mater Sci. 2013;48:2681–9.
- Li W, Xing Y, Wu Y, Wang J, Chen L, Yang G, Tang B. Study the effect of ion-complex on the properties of composite gel polymer electrolyte based on Electrospun PVdF nanofibrous membrane. *Electrochim Acta*. 2015;151:289–96.
- 48. Turner GA, Balasubramanian M. Investigations of the contributions to the tensile strength of weak particulate masses. *Powder Technol.* **1974**;*10*:121–7.
- 49. Devi PI, Ramachandran K. Dielectric studies on hybridised PVDF–ZnO nanocomposites. *J Exp Nanosci.* **2011**;*6*:281–93.
- Wang Y, Yang Y, Wang ZL. Triboelectric nanogenerators as flexible power sources. Flex Electron. 2017. https://doi.org/10.1038/ s41528-017-0007-8.
- Lee JP, Lee JW, Baik JM. The progress of PVDF as a functional material for triboelectric nanogenerators and self-powered sensors. *Micromachines*. 2018;9:532.
- Maity K, Mahanty B, Sinha TK, Garain S, Biswas A, Ghosh SK, Manna S, Ray SK, Mandal D. Two-dimensional piezoelectric MoS2-modulated nanogenerator and nanosensor made of poly(vinlydine Fluoride) nanofiber webs for self-powered electronics and robotics. *Energy Technol.* 2017;5:234–43.
- Khalifa M, Mahendran A, Anandhan S. Synergism of graphiticcarbon nitride and electrospinning on the physico-chemical characteristics and piezoelectric properties of flexible poly(vinylidene fluoride) based nanogenerator. J Polym Res. 2019;26:73.
- Dhakras D, Borkar V, Ogale S, Jog J. Enhanced piezoresponse of electrospun PVDF mats with a touch of nickel chloride hexahydrate salt. *Nanoscale*. 2012;4:752–6.
- Alam MdM, Ghosh SK, Sultana A, Mandal D. An effective wind energy harvester of paper ash-mediated rapidly synthesized ZnO nanoparticle-interfaced electrospun PVDF fiber. ACS Sustain Chem Eng. 2018;6:292–9.
- Polsongkram D, Chamninok P, Pukird S, Chow L, Lupan O, Chai G, Khallaf H, Park S, Schulte A. Effect of synthesis conditions on the growth of ZnO nanorods via hydrothermal method. *Phys B*. 2008:403:3713–7.
- 57. Wang G, Deng Y, Xiang Y, Guo L. Fabrication of radial ZnO nanowire clusters and radial ZnO/PVDF composites with enhanced dielectric properties. *Adv Funct Mater*. **2008**;18:2584–92.
- Zhang Y, Liu C, Liu J, et al. Lattice strain induced remarkable enhancement in piezoelectric performance of ZnO-based flexible nanogenerators. ACS Appl Mater Interf. 2016;8:1381–7.



- Hsu C-L, Su I-L, Hsueh T-J. Sulfur-doped-ZnO-nanospire-based transparent flexible nanogenerator self-powered by environmental vibration. RSC Adv. 2015;5:34019–26.
- Choi M-Y, Choi D, Jin M-J, Kim I, Kim S-H, Choi J-Y, Lee SY, Kim JM, Kim S-W. Mechanically powered transparent flexible charge-generating nanodevices with piezoelectric ZnO nanorods. *J Adv Mater.* 2009;21:2185–9.
- 61. Wang ZL, Song J. Piezoelectric nanogenerators based on zinc oxide nanowire arrays. *Science*. **2006**;312:242–6.
- Lanceros-Méndez S, Mano JF, Costa AM, Schmidt VH. FTIR and DSC studies of mechanically deformed β-PVDF films. *J Macro-mol Sci B*. 2001;40:517–27.
- Ye B, Pogreb R, Stanevsky O, Bormashenko E. Vibrational spectrum of PVDF and its interpretation. *Polym Test.* 2004;23:791–6.
- Salimi A, Yousefi AA. Analysis method: FTIR studies of β-phase crystal formation in stretched PVDF films. *Polym Test*. 2003;22:699–704.
- Martins P, Lopes AC, Lanceros-Mendez S. Electroactive phases of poly(vinylidene fluoride): determination, processing and applications. *Prog Polym Sci.* 2014;39:683–706.
- Rinaldo GJ, Cestari M. Effect of crystallization temperature on the crystalline phase content and morphology of poly(vinylidene fluoride). *J Polym Sci B Polym Phys.* 1994;32:859–70.
- Tamura M, Ogasawara K, Ono N, Hagiwara S. Piezoelectricity in uniaxially stretched poly(vinylidene fluoride). *J Appl Phys*. 1974;45:3768–71.
- Zhong G, Zhang L, Su R, Wang K, Fong H, Zhu L. Understanding polymorphism formation in electrospun fibers of immiscible Poly(vinylidene fluoride) blends. *Polymer*. 2011;52:2228–37.
- Ribeiro C, Sencadas V, Ribelles JLG, Lanceros-Méndez S. Influence of processing conditions on polymorphism and nanofiber morphology of electroactive poly(vinylidene fluoride) electrospun membranes. *Soft Mater.* 2010;8:274–87.
- Levi N, Czerw R, Xing S, Iyer P, Carroll DL. Properties of polyvinylidene difluoride–carbon nanotube blends. *Nano Lett.* 2004;4:1267–71.
- Shin YM, Hohman MM, Brenner MP, Rutledge GC. Electrospinning: A whipping fluid jet generates submicron polymer fibers. *Appl Phys Lett.* 2001;78:1149–51.
- Baji A, Mai Y-W, Wong S-C, Abtahi M, Chen P. Electrospinning of polymer nanofibers: effects on oriented morphology, structures and tensile properties. *Compos Sci Technol.* 2010;70:703–18.
- Hohman MM, Shin M, Rutledge G, Brenner MP. Electrospinning and electrically forced jets. I. Stability theory. *Phys Fluids*. 2001;13:2201–20.
- 74. Lim JY, Kim S, Seo Y. Enhancement of β-phase in PVDF by electrospinning. *AIP Conf Proc.* **2015**;1664:070006.
- Ho Kim G, Man Hong S, Seo Y. Piezoelectric properties of poly(vinylidene fluoride) and carbon nanotube blends: β-phase development. *Phys Chem Chem Phys.* 2009;11:10506–12.
- Ahn Y, Lim JY, Hong SM, Lee J, Ha J, Choi HJ, Seo Y. Enhanced piezoelectric properties of electrospun Poly(vinylidene fluoride)/Multiwalled carbon nanotube composites Due to High β-Phase formation in Poly(vinylidene fluoride). *J Phys Chem C*. 2013;117:11791–9.
- Nguyen VS, Rouxel D, Vincent B, Badie L, Santos FDD, Lamouroux E, Fort Y. Influence of cluster size and surface functionalization of ZnO nanoparticles on the morphology, thermomechanical and piezoelectric properties of P(VDF-TrFE) nanocomposite films. *Appl Surf Sci.* 2013;279:204–11.

- Spasova M, Manolova N, Markova N, Rashkov I. Superhydrophobic PVDF and PVDF-HFP nanofibrous mats with antibacterial and anti-biofouling properties. *Appl Surf Sci.* 2016;363:363–71.
- 79. Liu B, Zeng HC. Hydrothermal synthesis of ZnO nanorods in the diameter regime of 50 nm. *J Am Chem Soc.* **2003**;*125*:4430–1.
- Geng C, Jiang Y, Yao Y, Meng X, Zapien JA, Lee CS, Lifshitz Y, Lee ST. Well-aligned ZnO nanowire arrays fabricated on silicon substrates. Adv Funct Mater. 2004;14:589–94.
- Chen C, Kelder EM, Schoonman J. Functional ceramic films with reticular structures prepared by electrostatic spray deposition technique. *J Electrochem Soc.* 1997;144:L289–91.
- Hjiri M, El Mir L, Leonardi SG, Pistone A, Mavilia L, Neri G. Al-doped ZnO for highly sensitive CO gas sensors. Sens Actuator B Chem. 2014;196:413–20.
- 83. Dang Z-M, Fan L-Z, Zhao S-J, Nan C-W. Preparation of nanosized ZnO and dielectric properties of composites filled with nanosized ZnO. *Mater Sci Eng B.* **2003**;99:386–9.
- Pu X, Zha J-W, Zhao C-L, Gong S-B, Gao J-F, Li RKY. Flexible PVDF/nylon-11 electrospun fibrous membranes with aligned ZnO nanowires as potential triboelectric nanogenerators. *Chem Eng J.* 2020;398:125526.



Minji Kim received her BS from Yonsei University, Korea, and MS and Ph.D. from Cornell University, USA. At Cornell University, she researched electrospun piezoelectric nanofibrous materials for wearable applications. She is currently a Senior Scientist at AlgiKnit Inc. Her research interests are sustainable polymeric fibers, wearable fibrous materials, and nanotechnology.



Jintu Fan holds BSc from Donghua University, China and PhD and DSc from The University of Leeds, UK. He is currently Chair Professor and Head of Institute of Textiles and Clothing (ITC), Hong Kong Polytechnic University (PolyU). He served ITC as Assistant Professor, Associate Professor, Full Professor and Associate Head from 1996 to 2012. He then joined Cornell University as Chair and Vincent V. C. Woo Professor of the Department of Fiber Science and Apparel Design in the College of

Human Ecology, where he orchestrated the establishment of the Cornell Institute of Fashion & Fiber Innovation and was the founding Director of the institute. He returned to PolyU in 2018.

